Report as of FY2006 for 2006TX225B: "Arsenic Removal by Novel Nanoporous Adsorbents-Kinetics, Equilibrium, and Regenerability"

Publications

Project 2006TX225B has resulted in no reported publications as of FY2006.

Report Follows

Final Report

Arsenic Removal by Novel Nanoporous Adsorbents - Kinetics, Equilibrium, and Regenerability -

Submitted to
Texas Water Resources Institute

By:

Dongsuk Han,
Ph. D graduate student

Zachry Department of Civil Engineering
Environmental and Water Resources Division
Texas A&M University

Faculty Advisor:

Dr. Bill Batchelor,
Professor

Zachry Department of Civil Engineering
Environmental and Water Resources Division
Texas A&M University

May 2007

ABSTRACT

Arsenic contamination in groundwater is of major concern to many water treatment facilities in the world. Various treatment technologies have been applied to remove arsenic from drinking water. Among them, adsorption processes are often considered to be most effective forms of treatment for As(V), but they can be limited in their ability to remove As(III). To enhance removal efficiency of adsorption process for As(III) as well as As(V), this study has focused on developing highly ordered mesoporous silica solid (SBA-15) that can incorporate reactive titania sorption sites ($Ti_{(x)}$-SBA-15), and on synthesizing nanoporous titania (NT). XRD results showed that both $Ti_{(25)}$-SBA-15 and NT synthesized had surface property of anatase (TiO_2). From nitrogen adsorption/desorption tests, mesoporosity of these solids were observed by showing hysteresis loops which is representative of Type IV isotherm. However, TEM images showed that SBA-15 and $Ti_{(25)}$-SBA-15 have highly ordered hexagonal mesoporosity and titania nanostructured mesopores. However, NT has disordered wormhole-like mesopores that are caused by interparticle porosity. Based on q_{max} (μmol As/g) in the Langmuir isotherm, $Ti_{(25)}$-SBA-15 had more sorption capacity for As(III) than did $Ti_{(15,35)}$-SBA-15. It was also observed by FT-IR analysis that the peak intensity of the silanol (Si-OH) peak at 960 cm^{-1} was stronger for $Ti_{(25)}$-SBA-15. This indicates that $Ti_{(25)}$-SBA-15 has not exceeded its capacity to incorporate Ti. The rates of arsenic uptake were very fast and followed a bi-phasic sorption pattern where sorption was fast for the first 10 minutes, and then slowed until being almost completed within 200 minutes of contact. The Langmuir isotherm more accurately fitted experimental sorption data than did the Freundlich model. The order of maximum As(III) sorption capacity was NT (162 μmol/g) > $Ti_{(25)}$-SBA-15 (87 μmol/g) > $Ti_{(35)}$-SBA-15 (76 μmol/g) > $Ti_{(15)}$-SBA-15 (60 μmol/g). The order of sorption capacity for As(V) was NT (pH 9.5, 285 μmol/g) > NT (pH 7, 162 μmol/g) > $Ti_{(25)}$-SBA-15 (pH 4, 121 μmol/g) > $Ti_{(25)}$-SBA-15 (pH 7, 87 μmol/g) > NT (pH 4, 66 μmol/g) > $Ti_{(25)}$-SBA-15 (pH 9.5, 60 μmol/g). Distinct sorption maxima for As(III) removal were observed between pH 8 and pH 11 for NT and between pH 4 and pH 7 for $Ti_{(25)}$-SBA-15. The amount of As(V) adsorbed generally decreased as pH increased.

1. Introduction

Arsenic contamination in groundwater is serious threat to human health because of its toxicity and carcinogenicity. Arsenic contamination is found in many countries and has been caused by use of arsenical pesticides, activities related to mining, fallout from the atmosphere, and natural geologic weathering process [*1*]. In the US, arsenic has been ranked as the contaminant that poses the greatest risk to human health based on frequency of occurrence at NPL sites, toxicity, and potential for human exposure [*2*]. The toxicity and carcinogenicity of arsenic have compelled regulatory agencies in many countries to consider standard levels for arsenic in drinking water that are less than 10 ppb. Therefore, enhanced arsenic removal technologies are needed to meet these stringent standards for drinking water and to meet related standards for wastewater effluents.

Arsenite (As(III)) and arsenate (As(V)) are the oxidation states of arsenic that are generally found in subsurface environments. The distribution between different species of each valence state depends primarily on pH. Arsenous acid (H_3AsO_3) has pK_a values at 9.22, 12.13 and 13.40 while arsenic acid (H_3AsO_4) has pK_a values of 2.20, 6.97, and 11.53. In reduced environments at pH in the typical environmental pH range, nonionic arsenous acid (H_3AsO_3) is the primary species of arsenic [*3*]. In oxidized environments, on the other hand, two ionic arsenate species ($H_2AsO_4^-$ or $HAsO_4^{2-}$) exist, depending on the pH. Specifically, arsenite is more mobile, more toxic, and more difficult to remove due to its electro-neutrality.

The commonly applied processes for arsenic removal are chemical precipitation, co-precipitation, reverse osmosis, ion exchange, and oxidative filtration [*3*]. Adsorption is considered to be the most promising process, because of its safety, ease of handling and set-up, high removal efficiency with low cost, and potential for regeneration of materials [*4*]. Despite their wide availability, adsorption process may not be able to decrease As(III) concentrations to acceptable levels because of their physical limitations, although they are lowering As(V) concentration to

acceptable levels. Traditional adsorbents have a relatively low density of surface sites with an affinity for As(III), which leads to low removal efficiency. Also, their irregular physical structure makes it difficult for arsenic to easily access internal sorption sites. To overcome these disadvantages, this study proposed novel nanostructured adsorbent media for removal of both As(III) and As(V).

Nanostructured mesoporous materials studied in this research project are widely used in many industries because they have improved physical, chemical, and biological properties. These solid materials include an ordered structural frame work, high surface area, high density of surface functional groups, large pore volume, and the ability to incorporate catalytic components [*5-7*]. Nevertheless, applications of mesoporous materials to environmental technology have not been studied extensively. Therefore, the purpose of this study is to develop highly ordered nanostructured mesoporous adsorbents (NMAs) for removing both As(III) and As(V) from water to low concentrations. Two types of NMAs were produced and characterized. The characteristics of these NMAs for sorption of As(III) and As(V) were evaluated by kinetic and equilibrium tests.

2. Methodology

2.1 Synthesis of nanostructured mesoporous adsorbents (NMAs)

2.1.1 Mesoporous silica molecular sieves (SBA-15)

SBA-15 was synthesized by modifying the procedure described by Zhao et al [*8*]. A portion (4 g) of Pluronic P123 triblock copolymer (poly(ethylene oxide)-poly(propylene oxide)-poly(ethylene oxide), $EO_{20}PO_{70}EO_{20}$, Aldrich) was dissolved in 2 M HCl solution and mixed for 30 minutes at room temperature. Then, 9 mL of tetraethyl orthosilicate (TEOS) were added and the mixture stirred using a rotary mixer for 20 hours at 45 °C. The resulting gel was allowed to age for 48 hours at 80 °C. The solid product was then filtered from the mixture with a 0.45 μm filter, washed with distilled water, and dried at room temperature. Finally, the solid was calcined at 550 °C for 6 hours to remove the polymer. Figure 1 shows synthesis procedure of SBA-15.

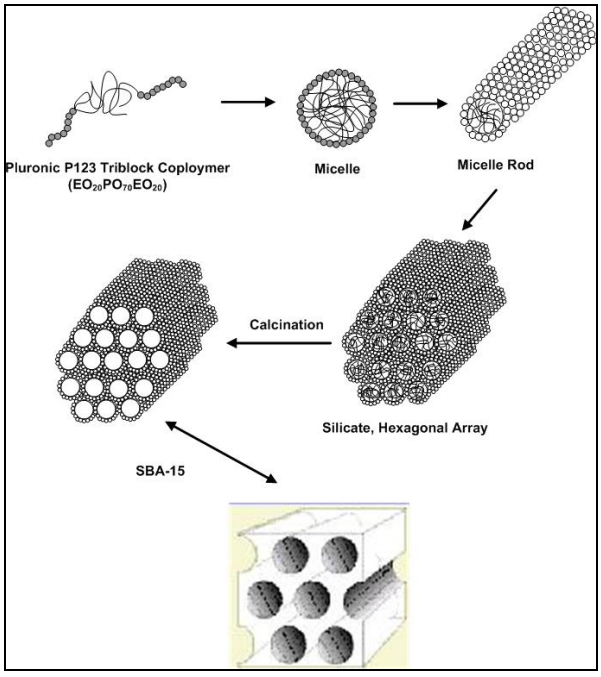

Figure 1. Schematic diagram for SBA-15 synthesis procedure

2.1.2 Nanoporous titania incorporated with SBA-15 ($Ti_{(x)}$-SBA-15)

Titanium was grafted on SBA-15 by following the general incipient impregnation method [*9*]. First, 1 g of SBA-15 was pretreated at 120 °C for 3 hours to remove adsorbed water. The pretreated SBA-15 was dispersed in 100 mL of anhydrous solvent (i.e., ethanol or isopropyl alcohol, Aldrich 99.8 %) and then the appropriate amount of titanium isopropoxide ($Ti(OPr)_4$, Aldrich, 97 %) was slowly added to achieve the desired loading of titanium. The mixture was stirred for 24 hours, followed by filtration and washing with ethanol. Then, the resulting solids were dried at 90 °C for 3 hours and finally calcined in furnace at 550 °C for 6 hours. The NMA produced was identified as "$Ti_{(x)}$-SBA-15", where the subscript x stands for the weight ratio of Ti to SBA-15.

2.1.3. Nanoporous titania (NT)

Nanoporous titania (NT) adsorbent was prepared with the procedure described by Huang et al [*10*]. A portion (6.65 mL) of titanium (IV) butoxide was added to ethanol as an anhydrous solvent with a weight ratio of 1/7 and then the system was vigorously stirred. After 30 min, 0.96 mL of 0.28 M phosphoric acid was added and stirred for 3 hours. Then, 72.4 mL of distilled water was added, the mixture was continuously stirred for 2 hours, and vaporized at 80 °C by an evaporator. The resulting solids were washed with ethanol, dried at 80 °C for 6 hours, and calcined at 550 °C for 6 hours. Figure 2 shows the synthetic final products for SBA-15, Ti-SBA-15, and NT.

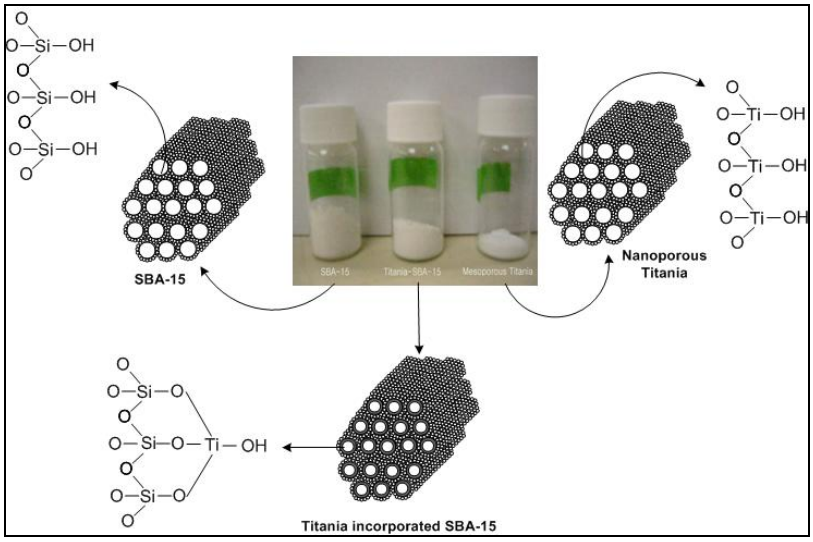

Figure 2. Schematic diagram of SBA-15, Ti-SBA-15, and NT

2.2 Kinetics experiment

Kinetic experiments for As(III) and As(V) uptake were performed by using a solids concentration of 1 g/L at pH 4, 7, and 9.5 in a solution of NaCl as background electrolyte to give an ionic strength of 0.01 M. The suspension was mixed for 2 hours and then that amount of arsenic stock solution was added to achieve an initial arsenic concentration of 13.3 μM. The desired initial pH was adjusted by adding 0.5 M HCl or 0.5 M NaOH. The reaction vessel was mixed by a reciprocal shaker with 200 rpm to promote arsenic uptake. At specified sampling times, approximately 10 mL of solid suspension was filtered by cellulose nitrate membrane filter (Whatman®) with a pore size of 0.2 μm. Approximately 12 samples were taken over the time period of 5 min to 1 day. All filtered samples were placed into an anaerobic chamber to avoid arsenic oxidation or pH change until atomic absorption spectroscopy (AAS) analysis.

2.3 Equilibrium experiment

Equilibrium experiments were conducted to evaluate sorption capacity of each adsorbent for As(III) and As(V). To start each equilibrium test, 10 mL of 2 g/L of adsorbent suspension was added to 20 mL of reaction vessels and then 10 mL of a mixture of de-ionized water and arsenic stock solution (200 ppm) was added to reach a solid concentration of 1 g/L and specified initial arsenic concentration. The desired pH was adjusted using 0.5 HCl or 0.5 M NaOH. The reaction vessels were mixed by a reciprocal shaker at 200 rpm. After 24 hours of reaction, all samples were filtered using cellulose nitrate membrane filter (Whatman®) with pore size of 0.2 μm. All filtered samples were placed into an anaerobic chamber to avoid arsenic oxidation or pH change until atomic absorption spectroscopy (AAS) analysis. In order to describe arsenic removal onto solids, two equilibrium isotherms were applied to the experimental data. One is the Langmuir model, which can be represented by

$$q_e = \frac{q_{\max} b C_e}{1 + b C_e} \qquad (1)$$

Where q_e is the equilibrium concentration of target compound on the solid (μmol/g), q_{max} is maximum concentration of target compound on the solid (*i.e.*, maximum sorption capacity, μmol/g), b is the Langmuir isotherm parameter (L/μmol). The other model is the Freundlich isotherm.

$$q_e = k_f C_e^{1/n} \qquad (2)$$

Where k_f is the Freundlich constant that is related to the capacity of adsorbent to adsorb adsorbate ($\mu mol^{1-1/n} \cdot L^{1/n}/g$) and n is also the Freundlich constant that expresses the affinity of adsorbate to the surface. As an extended equilibrium experiment, arsenic adsorption envelopes were conducted as a function of pH. Specific amounts of solid suspension and arsenic stock solution were added to 20 mL of reaction vessels to reach specified initial arsenic concentrations and a solids concentration of 1 g/L. The initial solution pH was adjusted to values between pH 4 and pH 12 with a pH increment of 0.5 unit by adding 0.5 HCl or 0.5 M NaOH. The samples were filtered and stored using the procedure described for kinetic experiments.

2.4 Arsenic analysis

Arsenic was analyzed with a model Solar M6 atomic absorption spectrometer equipped with a model V90 continuous hydride generator (Thermo Elemental). The procedure for measuring total arsenic (As(III) + As(V)) was based on Standard Method 3114C, which is a continuous hydride generation/atomic absorption spectrometer (HGAAS) method [*11*]. Total arsenic is determined by mixing a sample flow of 7 mL/min with an equal flow of strong acid (6 M HCl) and a 3.5 mL/min flow of sodium borohydride. With these flows and pH conditions, both As(III) and As(V) can be reduced by borohydride to arsine gas [*12*]. The arsine is transferred by argon gas with a 250 mL/min flow to the flame AA, where its absorbance is determined and used to calculate the arsenic concentration using a standard calibration curve.

2.5 XRD analysis

X-ray diffractograms were collected using a Riga automated X-ray diffractometer using CuKα radiation (40 kV, 20 mA) with a 0.05^o step size and 3s step time over the range $6^o < 2\theta < 60^o$.

2.6 Nitrogen adsorption isotherm

Nitrogen adsorption experiments were performed on a Micrometrics ASAP 2010 micropore system using approximately 0.1 g of sample. The samples were degassed under vacuum at room temperature for 2 hours, then at 100^{o}C for 4 hours, and then at 300^{o}C for overnight prior to analysis. The surface area was calculated by the BET method. The micropore and mesopore volumes were determined using the alpha s-method [*13-14*]. The mesopore size distributions were calculated from the adsorption branch of the isotherm using the BJH method with a modified equation for the statistical film thickness [*15-16*].

2.7 TEM analysis

Transmission electron microscopy (TEM) was performed using a JEOL 2010 microscope with a lanthanum hexaboride filament and an excitation voltage of 200 kV. The solid samples were washed with ethanol (99.99 %, Aldrich) and dried as soon as possible, and then transferred to a 400-mesh copper grid, followed by dispersion of the solids by sonication.

2.8 FTIR analysis

Fourier transform infrared (FTIR) spectra were measured using the KBr wafer technique. Samples of 1 g were dried and KBr was mixed with 0.02 g portions of the dried sample. Appropriate amounts of the prepared samples were moved to sample chamber and their FTIR peaks were recorded in transmission mode using a Perkin Elmer 2000 FTIR spectrophotometer. A total 64 scans were collected with a triglycine sulfate (TGS) detector at a resolution of 1 cm^{-1}.

3. Results and discussion

3.1 XRD patterns of NMAs

Figure 3 shows the wide-angle XRD pattern of NT. Comparison of the measured d-spacings to the values in JCPDS card (i.e., 3.516, 1.892, 2.378, 1.700, 1.666, and 1.480 nm) shows that they are the same as those for anatase, which is a crystalline form of TiO_2. Figure 4 shows that the XRD patterns of SBA-15 and titanium-incorporated SBA-15 are very similar to those reported by other studies, indicating that the broad XRD reflection peak at 23^{o} is caused by the very small size of the solid [*17-18*]. Also, Figure 4 shows that the highest peak for $Ti_{(25)}$-SBA-15 is closest to 2θ equal to 25^{o}, which is similar to that observed for anatase, even though peaks for $Ti_{(15,35)}$-SBA-15 are also near 2θ equal to 25^{o} . In contrast, rutile has its highest peak at about 2θ equal to 54^{o} or 56^{o}. Therefore, it can be expected that $Ti_{(25)}$-SBA-15 has properties that are similar to those of anatase.

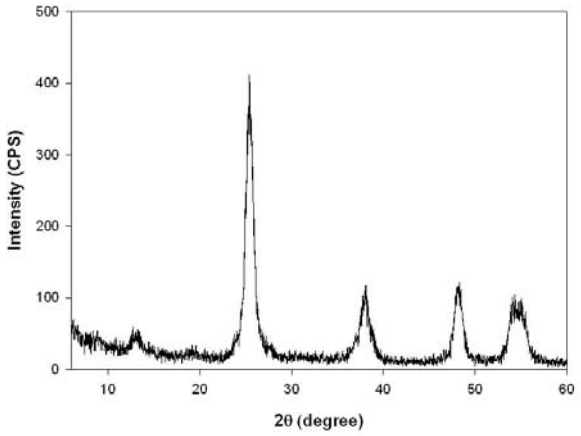

Figure 3. High angle XRD patterns for NT

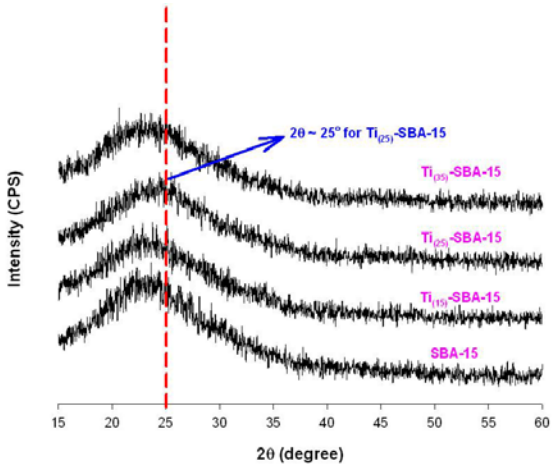

Figure 4. High-angle XRD patterns for SBA-15, $Ti_{(15)}$-SBA-15, $Ti_{(25)}$-SBA-15, and $Ti_{(35)}$-SBA-15 samples.

3.2 Porosity characterization of NMAs

Figure 5 shows nitrogen adsorption-desorption isotherms for NT and $Ti_{(25)}$-SBA-15. They follow the typical irreversible type IV model as designated by IUPAC (International Union of Pure and Applied Chemistry) classification [*14*]. These NMAs have a H1 hysteresis loop, which is representative of mesopores. The sharpness of the inflection step for $Ti_{(25)}$-SBA-15 was greater than that of NT, so it appears that $Ti_{(25)}$-SBA-15 has more uniformity in its mesopores than NT. Figure 6 shows the distribution of pore volume in these NMAs. It provides further evidence of the differences in porosities. It shows a sharp peak at 7.3 nm for $Ti_{(25)}$-SBA-15, whereas NT had broad peak at 9.4 nm. The specific surface areas (A_{BET}) and specific pore volumes (V_{BJH}) for NT were 114 m^2/g and 0.28 cm^3/g, respectively, and for $Ti_{(25)}$-SBA-15 were 588 m^2/g and 0.78 cm^3/g, respectively.

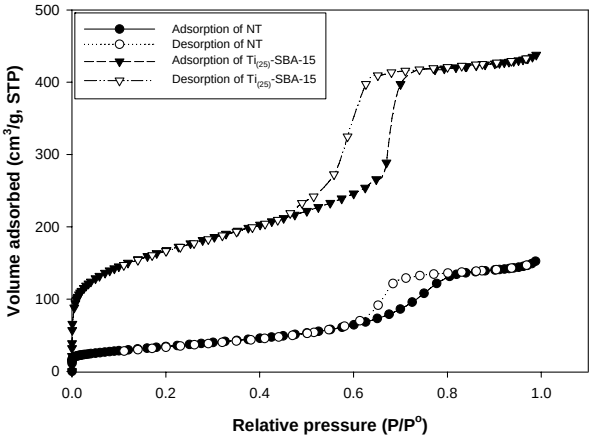

Figure 5. N_2 adsorption-desorption isotherms for NT and $Ti_{(25)}$-SBA-15

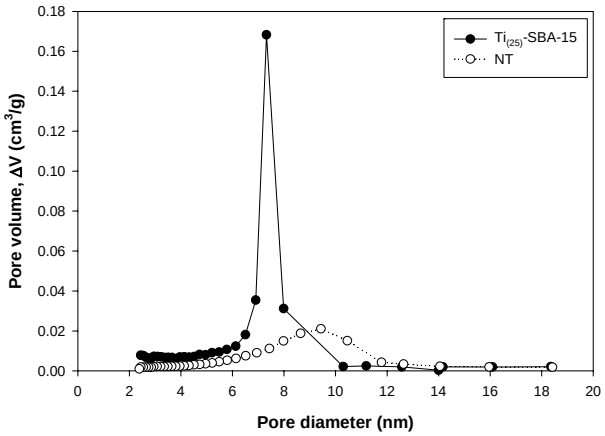

Figure 6. Pore size distribution for NT and $Ti_{(25)}$-SBA-15

3.3 Transmission element microscopy (TEM)

Figure 8 shows that SBA-15 and $Ti_{(25)}$-SBA-15 have highly ordered hexagonal pores with diameters of approximately 10 nm,. However, NT has a disordered wormhole-like pore structure with pore sizes in the range of 10 nm to 20 nm. This agrees with Huang et al. who reported that NT was formed by the agglomeration of TiO_2 nanoparticles and had its mesoporosity caused by interparticle porosity rather than intraparticle porosity [*10*]..

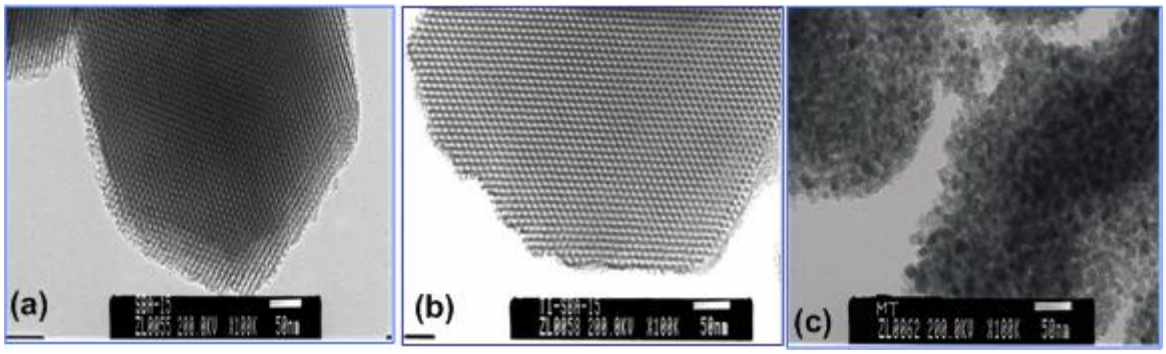

Figure 8. TEM images of a) SBA-15, b) $Ti_{(25)}$-SBA-15, and c) NT.

3.4 FT-IR spectroscopy analysis

Figure 8 shows FT-IR spectra for several NMA. The spectra show three peaks at 445, 795, and 1070 cm^{-1}, indicating rocking, bending (or symmetric stretching), and asymmetric stretching of the tetrahedral oxygen atoms in the SiO_2 structure [*19*]. In addition, the peak at 960 cm^{-1} is assigned to the silanol group (Si-OH) in the framework of SBA-15 by the stretching of nonbridging oxygen atoms [*19*]. As the extent of titanium incorporation increases, the peak at 960 cm^{-1} gradually decreases because of the interaction between titanium and the silanol groups. This peak can be also assigned to Ti-O-Si stretching vibration [*20*]. From this result, we can postulate that SBA-15 can incorporate more titanium into their frameworks, because the presence of peaks at 960 cm^{-1} indicates that the silanol groups have not been completely consumed. Furthermore, the decrease in intensity of the peak at 1070 cm^{-1} in $Ti_{(35)}$-SBA-15 indicates that O-Si-O bonding in the mesoporous SBA-15 framework was decreased by attack of titanium. Thus, excessive impregnation of titanium can destroy the pore structure of SBA-15. The peaks at around 3600 and 1615 cm^{-1} can be attributed to the stretching vibration of hydroxyl and water, caused by humidity

of KBr used as a blank sample or humidity incorporation into sample in the process of sample preparation [*20*].

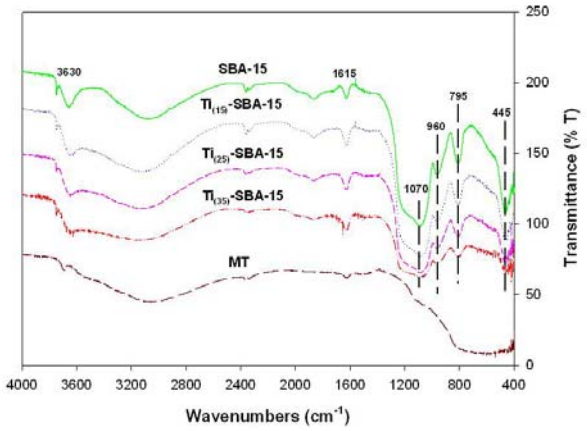

Figure 8. FT-IR spectra of SBA-15, $Ti_{(15,25,35)}$-SBA-15, and NT

3.5 Kinetics for arsenic uptake

Arsenic sorption kinetics by $Ti_{(25)}$-SBA-15 and NT were investigated in a batch system at three different initial pH (4, 7, 9.5). Figure 9 shows the experimental results for As(III) uptake by $Ti_{(25)}$-SBA-15 and NT where the solid concentration was 1 g/L and the initial As(III) concentration was 13.3 μM. Figure 9 (a) and (b) shows that adsorption of As(III) onto both adsorbents initially was very rapid with most being removed within the first 10 minutes of contact, and later was slower. This biphasic kinetics could be caused by transformation of arsenic species adsorbed or by other environmental factors. Specifically, the slower sorption reaction could be attributed to surface precipitation or polymerization, diffusion into interparticle or intraparticle pores, or changes in the type of surface complex (*i.e.*, monodentate adsorption followed by bidentate complex) as reported by other studies [*21-22*]. In this study, it could be postulated that slower adsorption of arsenic might be controlled by intraparticle diffusion because NMAs have a lot of pores and channels. The extent of As(III) uptake by NT increased with increasing pH over the range investigated, whereas the highest level of As(III) removal by $Ti_{(25)}$-SBA-15 was observed at pH 7. The amount adsorbed at pH 7 was and initially much greater than adsorbed at pH 4. However, after a longer time of reaction, the amount removed at pH 4 became nearly as high as that at pH 7. At pH 9.5, the removal efficiency of NT for As(III) was more than three times greater than that of $Ti_{(25)}$-SBA-15.

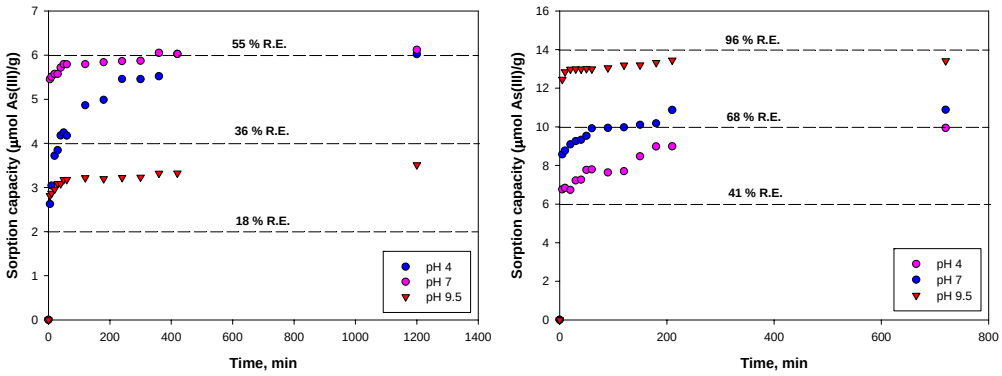

Figure 9. As(III) uptake rate by (a) $Ti_{(25)}$-SBA-15 (left) and (b) NT (right) as a function of pH

The kinetic experiments for As(V) removal were conducted in a similar manner. Figure 10 (a) and (b) show that the amount of As(V) removed depends strongly on solution pH. At lower pH, higher As(V) adsorption was observed, which can be caused by electrostatic attraction between As(V) species and positive surface functional groups. While at high pH, lower removal of As(V) was observed and this could be caused by electrostatic repulsion. In spite of the similar trends of As(V) removal by each adsorbent over the pH range investigated, the extent of As(V) uptake at a specified pH was very different. For instance, As(V) at pH 4 was completely removed by $Ti_{(25)}$-SBA-15, whereas only 91 % of As(V) was adsorbed by NT. However, at other pH, the extent of As(V) uptake by NT was much higher than that by $Ti_{(25)}$-SBA-15.

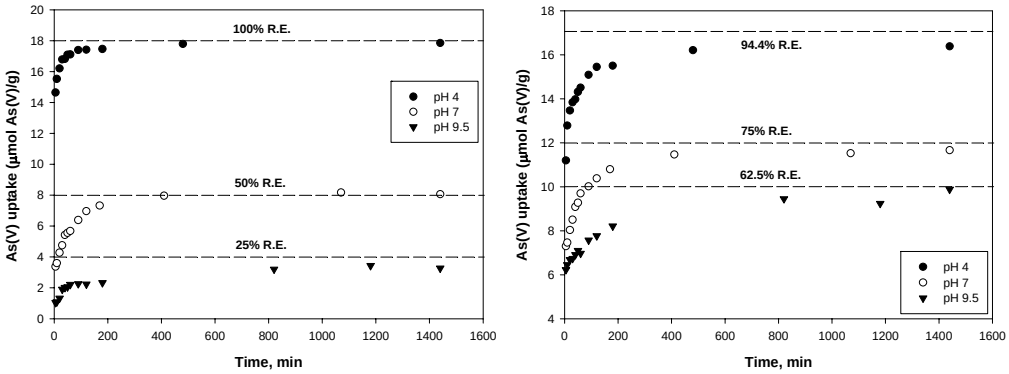

Figure 10. As(V) uptake rate by (a) $Ti_{(25)}$-SBA-15 (left) and (b) NT (right) as a function of pH

3.6 Nonlinear Equilibrium for arsenic uptake

Figure 11 shows As(III) adsorption isotherms for $Ti_{(15,25,35)}$-SBA-15 and NT with Figure 11(a) showing the Langmuir isotherm and Figure 11 (b) showing the Freundlich isotherms. These isotherms were obtained by non-linear regression using data for adsorption of As(III). Table 1 shows the fitting parameters for these isotherm models and the sum of squared residuals (SSR). These results show that the maximum sorption capacity for As(III) decrease as follows; NT (162 µmol/g) > $Ti_{(25)}$-SBA-15 (87 µmol/g) > $Ti_{(35)}$-SBA-15 (76 µmol/g) > $Ti_{(15)}$-SBA-15 (60 µmol/g). The SSR values in Table 1 show that the Langmuir isotherm model provided a better fit than the Freundlich isotherm model for both adsorbents. These results indicate that the optimal weight ratio of Ti to SBA-15 for As(III) adsorption is 25 %. As(III) sorption capacity decreased when the incorporation ratio increased from 25% to 35%, possibly due to incorporation of Ti into the silica

framework. Ti that is in the silica framework would not function as reactive sorption sites for As(III) removal. Similar results have been observed in other studies that investigated $La_{(x)}$-SBA-15, $Al_{(x)}$-SBA-15, and $Fe_{(x)}$-SBA-15 [*23*]. In addition, NT had a higher sorption capacity than $Ti_{(25)}$-SBA-15, by a factor of 1.7.

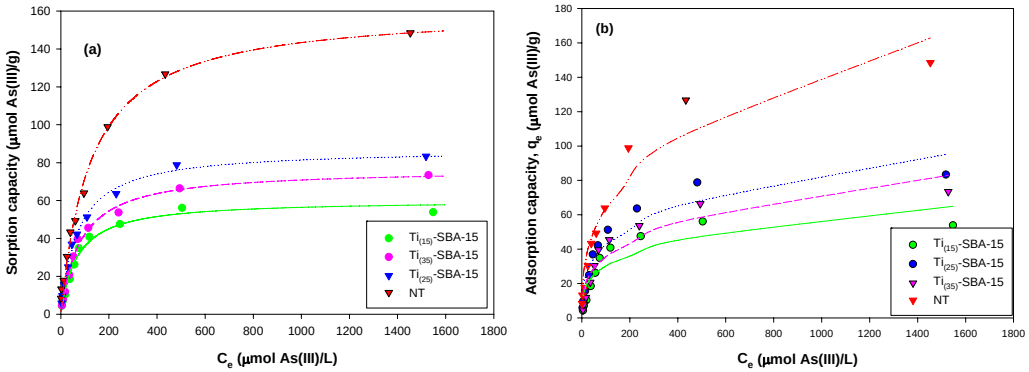

Figure 11. As(III) adsorption isotherm by $Ti_{(15,25,35)}$-SBA-15 and NT with solid concentration = 1g/L. The nonlinear fitting curves are obtained from (a) the Langmuir and (b) Freundlich isotherm model.

Table 1. Comparison of isotherm parameters ±95% confidence levels for As(III) adsorption

	$Ti_{(15)}$-SBA-15	$Ti_{(25)}$-SBA-15	$Ti_{(35)}$-SBA-15	NT
Langmuir				
b (L/µmol)	0.014±0.004	0.014±0.003	0.013±0.003	0.008±0.002
Q_{max} (µmol/g)	60±6	87±5	76±5	162±14
SSR	60	41	42	250
Freundlich				
K_f ($\mu mol^{1-1/n} \cdot L^{1/n}/g$)	8.3±6.4	11±6.3	8.6±5.5	12.7±6.8
n	3.6±1.7	3.4±1.1	3.3±1.1	2.8±0.6
SSR	650	710	600	1200

Experiments were conducted at three pH values (pH 4, 7, 9.5) in order to investigate the effect of pH on maximum sorption capacity of each adsorbent for As(III) and As(V). Figures 12, 13, 14, and 15 show adsorption isotherms fitted by the Langmuir and Freundlich model. Adsorption isotherm parameters are summarized in Table 2 and 3. In the case of As(III) removal, we can determine the order of maximum sorption capacity to be: NT (pH 9.5, 285 µmol/g) > NT (pH 7, 162 µmol/g) > $Ti_{(25)}$-SBA-15 (pH 4, 121 µmol/g) > $Ti_{(25)}$-SBA-15 (pH 7, 87 µmol/g) > NT (pH 4, 66 µmol/g) > $Ti_{(25)}$-SBA-15 (pH 9.5, 60 µmol/g). In addition, at all pH except for pH 9.5, the Langmuir model for As(III) sorption provided a better fit than the Freundlich model as measured by SSR.

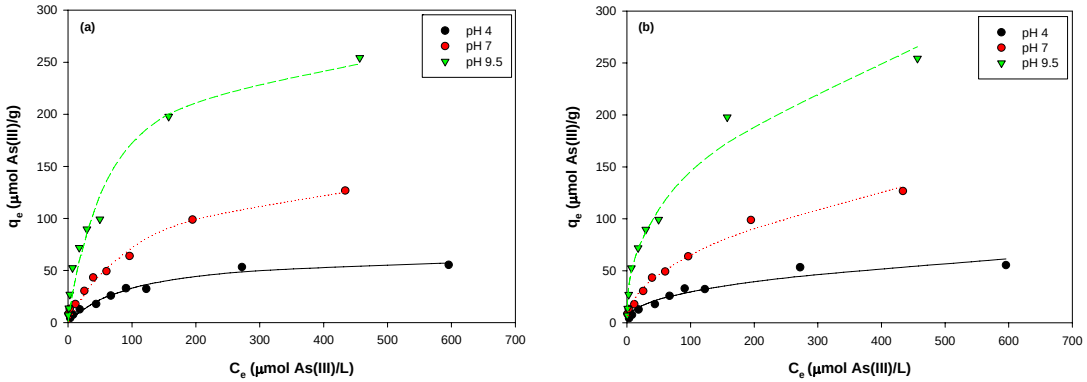

Figure 12. As(III) adsorption isotherms by NT as function of pH that are fitted to (a) the Langmuir and (b) Freundlich model by non-linear regressions using MATLAB®

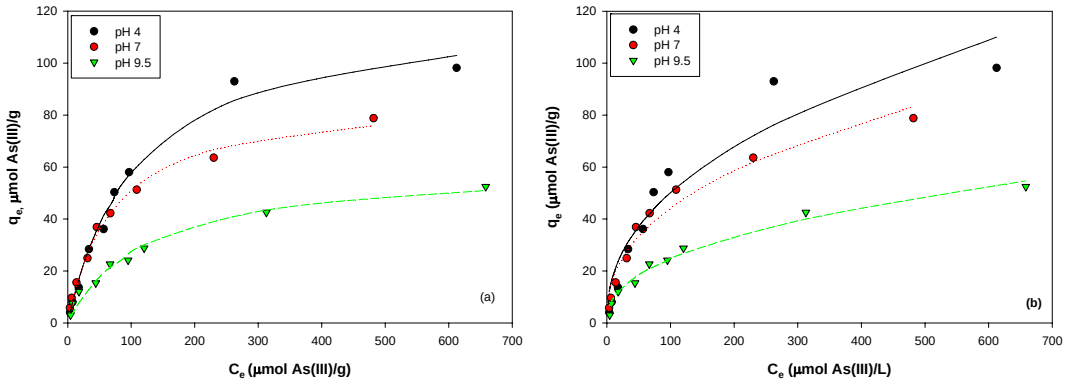

Figure 13. As(III) adsorption isotherms by $Ti_{(25)}$-SBA-15 as function of pH that are fitted to (a) the Langmuir and (b) Freundlich model by non-linear regressions using MATLAB®

Table 2. Comparison of As(III) adsorption isotherm parameters as a function of pH

NMAs	pH	***Langmuir***			***Freundlich***		
		b (L/µmol)	q_{max} (µmol/g)	SSR	k_f(µmol$^{1-1/n}$·L$^{1/n}$/g)	n	SSR
NT	4	0.01±0.004	66±11	69	4.71±2.86	2.5±0.7	167
	7	0.008±0.002	162±14	250	12.7±6.8	2.8±0.6	1200
	9.5	0.015±0.008	285±52	1705	22.4±7.8	2.48±0.4	1052
$Ti_{(25)}$-SBA-15	4	0.009±0.0027	121±14	117	6.79±5.34	2.3±0.7	783
	7	0.014±0.003	87±5	41	11±6.3	3.4±1.1	710
	9.5	0.0083±0.0031	60±9	48	3.59±1.37	2.4±0.4	38

The order of maximum sorption capacity for As(V) is: $Ti_{(25)}$-SBA-15 (pH 4, 193 µmol/g) > NT (pH 4, 173 µmol/g) > NT (pH 4, 116 µmol/g) > $Ti_{(25)}$-SBA-15 (pH 7, 72 µmol/g) > NT (pH 9.5, 56 µmol/g) > $Ti_{(25)}$-SBA-15 (pH 9.5, 30 µmol/g). Except for pH 9.5, the Langmuir model for As(V) provides the best fit to experimental isotherm data as measured by the SSR.

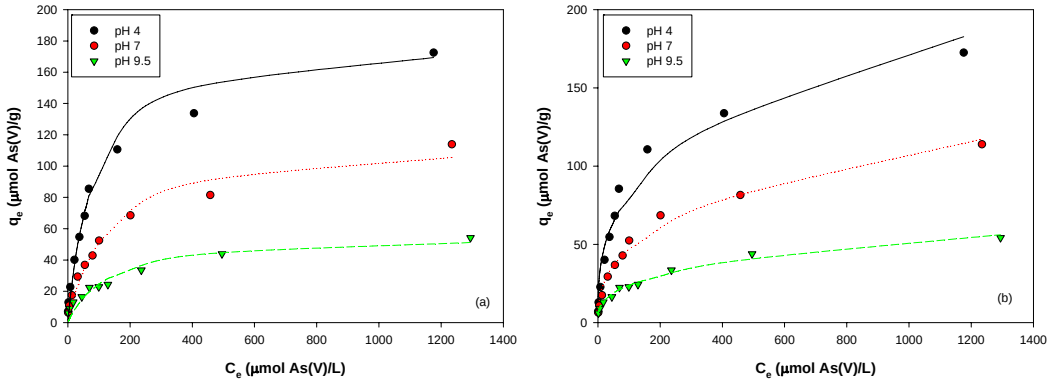

Figure 14. As(V) adsorption isotherms by NT as function of pH that are fitted to (a) the Langmuir and (b) Freundlich model by non-linear regressions using MATLAB

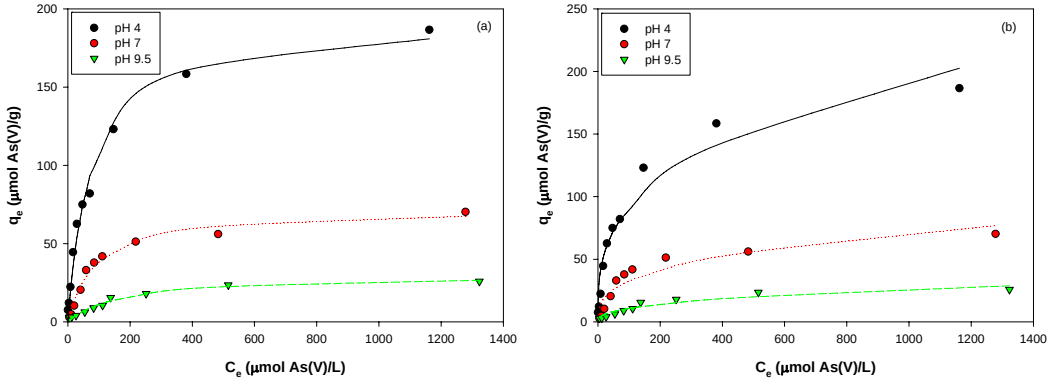

Figure 15. As(V) adsorption isotherms by $Ti_{(25)}$-SBA-15 as function of pH that are fitted to (a) the Langmuir and (b) the Freundlich model by non-linear regressions using MATLAB

Table 3. Comparison of As(V) adsorption isotherm parameters as a function of pH

NMAs	pH	***Langmuir***			***Freundlich***		
		b (L/µmol)	q_{max} (µmol/g)	SSR	k_f ($\mu mol^{1-1/n} \cdot L^{1/n}/g$)	n	SSR
NT	4	0.0128±0.0038	173±16	449	17.8±6.9	3.03±0.59	1013
	7	0.008±0.003	116±17	331	8.8±2.4	2.75±0.33	159
	9.5	0.0078±0.004	56±11	155	5.1±1.1	2.99±0.31	26
$Ti_{(25)}$-SBA-15	4	0.0081±0.0049	193±17	443	20.5±9.1	3.08±0.71	1649
	7	0.0031±0.0017	72±7.0	82	6.9±4.7	2.98±1.02	549
	9.5	0.0041±0.0013	30±4.0	15	1.85±1.27	2.62±0.76	55

3.7 Arsenic adsorption envelopes

To investigate the effect of pH and total As(III) concentration on the extent of adsorption onto solids over pH, three different As(III) concentration (*i.e.*, 7.82, 14.4, and 45.6 µM) were chosen. Figure 16(a) shows As(III) adsorption envelopes for NT in which a maximum is observed around pH 8-11. The percentage of As(III) adsorbed decreases with increasing total As(III) concentration. Figure 16(b) shows that As(III) removal by $Ti_{(25)}$-SBA-15 was somewhat constant over the pH range between pH 4 and pH 7, but decreased as pH increased about pH 8.5. The decrease as high pH may be caused by increased electrostatic repulsion between negative arsenite species

($H_2AsO_3^-$) and negative surface functional groups. Figure 17 (a) and (b) show the effect of total As(V) concentration on the extent of adsorption by NT and $Ti_{(25)}$-SBA-15. As shown in Figure 17(a), As(V) adsorption was pH dependent and the extent of As(V) adsorption decreased with increasing total As(V) concentration over all pH values investigated. Figure 17(b) shows that As(V) sorption to $Ti_{(25)}$-SBA-15 was more strongly dependent on pH rather than was sorption of As(III). As(V) adsorption to NT showed the highest percent adsorbed at low pH, compared to As(III) which showed decreasing removal at the lowest pH.

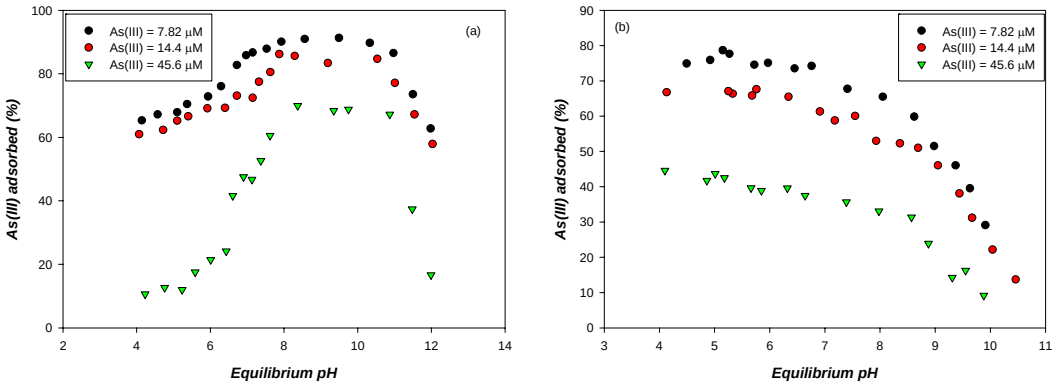

Figure 16. Adsorption envelope of As(III) by (a) NT and (b) $Ti_{(25)}$-SBA-15 as a function of pH; Solid concentration = 1 g/L, ionic strength = 0.01 M as NaCl, equilibration time = 24 hrs, total As(III) concentration added = 7.82, 14.4, and 45.6 µM, respectively.

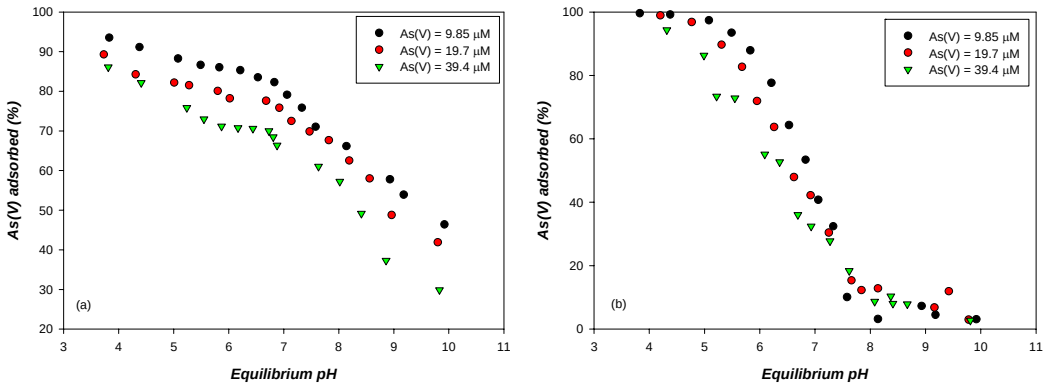

Figure. 17. Adsorption envelope of As(V) by (a) NT and (b) $Ti_{(25)}$-SBA-15 as a function of pH; solid concentration = 1 g/L, ionic strength = 0.01 M as NaCl, equilibration time = 24 hrs, total As(V) concentration added = 9.85, 19.7, and 39.4 µM, respectively.

4. Conclusions

Both As(III) and As(V) showed rapid removal during the first 10 minutes and then slower sorption until 200 minutes. After 24 hours of reaction, the extent of arsenic removal by $Ti_{(25)}$-SBA-15 and NT and how they were affected by pH were observed to be different. In the case of $Ti_{(25)}$-SBA-15, the amount of As(III) uptake became greater as pH shifted to pH 4 or pH 7, while in the case of NT, increasing pH enhanced As(III) sorption capacity over the entire range. NT had a higher equilibrium As(III) sorption capacity than $Ti_{(25)}$-SBA-15 over all pH ranges investigated. For As(V) uptake, high sorption capacity was observed at low pH, probably due to strong

electrostatic attraction. The extent of As(V) sorption onto both solids decreased with increasing pH.

Adsorption data for both As(III) and As(V) on $Ti_{(25)}$-SBA-15 and NT were more accurately modeled by the Langmuir isotherm than by the Freundlich isotherm. These results support the hypothesis that the affinity of the adsorbate for the surface sorption sites of NMAs is similar and that there is a maximum sorption capacity. Thus, the surface sorption sites on $Ti_{(25)}$-SBA-15 and NT have similar affinities for As(III) and As(V). However, pH can affect the maximum sorption capacity (q_{max}, μmol As/g) of each solid for As(III) and As(V). For As(III) sorption onto NT, higher sorption capacity was observed at pH 7 to 9.5, whereas for As(III) sorption onto $Ti_{(25)}$-SBA-15, higher capacities were seen at low pH. At environmental pH conditions, it could be expected that NT can achieve higher As(III) removal. In the case of As(V) removal, both solids had higher As(V) removal capacity at low pH and this is probably due to electrostatic attraction.

The extent of arsenic adsorption onto $Ti_{(25)}$-SBA-15 and NT showed a regular pattern with pH. This pattern was not affected by total arsenic concentration, but the percentages of As(III) and As(V) adsorbed decreased with increasing total arsenic concentration. Optimal pH ranges for As(III) removal were between pH 8 and pH 11 for NT and between pH 4 and pH 7 for $Ti_{(25)}$-SBA-15. Maximum removal efficiencies for As(V) by $Ti_{(25)}$-SBA-15 was observed in the pH range between pH 4 and pH 7 and the maximum for NT was close to pH 4. However, at environmental pH near pH 7 to pH 8, the extent of removal efficiencies for As(III) and As(V) by NT was greater than those by $Ti_{(25)}$-SBA-15. Consequently, it can be concluded that at environmental pH, NT could be a better adsorbent for removal of both As(III) and As(V).

The incorporation ratio of titanium that resulted in the highest maximum adsorption capacities was 25 %, *i.e,* $Ti_{(25)}$-SBA-15. Also, analyses by XRD, TEM, and FT-IR provided evidence that $Ti_{(25)}$-SBA-15 is a selective adsorbent with nanostructured titania surface properties. XRD analysis indicated that the peaks of synthetic NT were in accordance with those of anatase. In addition, nitrogen adsorption/desorption results showed that SBA-15, $Ti_{(25)}$-SBA-15, and NT follow typical irreversible type IV model as designated by IUPAC, which is indicative of mesoporous materials. Based on TEM results, however, the mesopores of NT could be related to interparticle porosity, unlike SBA-15 and $Ti_{(25)}$-SBA-15 which showed a highly regular hexagonal intraparticle porosity.

5. Research in the future works

We will continue to conduct experiments and develop theoretical mechanisms for arsenic removal to achieve the following objectives.

1) Develop sorption kinetics models to describe adsorptive and diffusive sorption removal mechanisms, and to predict sorption removal rates
2) Develop modified equilibrium models to predict sorption capacity more precisely
3) Determine optimum solution conditions as affected by competing anions (e.g., PO_4^{3-} and SO_4^{2-})
4) Characterize electrostatic surface properties of solids by potentiometric titration or electrophoretic mobility
5) Develop surface complexation model (SCM) using computer program software such as FITEQL and V-MINTEQ
6) Determine regenerability of solids for arsenic removal to predict life-cycle and cost-effectiveness

6. References

1. Waltham, C.A. and Eick, M.J. (2002) "Kinetics of Arsenic Adsorption on Goethite in the Presence of Sorbed Silicic Acid", *Soil Sci. Soc. Am. J.* **66**, 818-825.
2. US DOHHA. (2005) "CERCLA Priority List of Hazardous Substances that will be the Subject of Toxicological Profiles and Support Document", ATSDR. p44.
3. O'Neil, P. (1995) "Arsenic" In: Heavy Metals in Soil. Alloway ed., John Wiley and Sons, New York, NY.
4. Zhang Y., Yang, M., and Huang, X. (2003) "Arsenic(V) Removal with a Ce(IV)-Doped Iron Oxide Adsorbent", *Chemosphere*. ***51***, 945-952.
5. Kim, Y., Kim, C., Choi, I., Rengaraj, S., and Yi, J. (2004) "Arsenic Removal Using Mesoporous Alumina Prepared via a Templating Method", *Environ. Sci. Technol.* ***38***, 924-931.
6. Jang, M., Shin, E.W., Park, J.K., and Choi, S.I. (2003) "Mechanisms of Arsenate Adsorption by Highly-Ordered Nano-Structured Silicate Media Impregnated with Metal Oxides", *Environ. Sci. Technol.* ***37.*** 5062-5070.
7. Fryxell, G.E., Liu, J., Hauser, T.A., Nie, Z., Ferris, K.F., Mattigod, S., Gong, M., and Hallen, R.T. (1999) "Design and Synthesis of Selective Mesoporous Anion Traps", *Chem. Mater.* ***11***, 2148-2154.
8. Zhao, D., Feng, J., Huo. Q., Melosh, N., Fredrickson, G.H., Chmelka, B.F., and Stucky, G.D. (1998) "Triblock Copolymer Syntheses of Mesoporous Silica with Periodic 50 to 300 Angstrom Pores", *Science*. **279**, 548-552
9. Luan, Z., Maes, E-M., van der Heide, P.A.W., Zhao, D., Czernuszewicz, R.S.,and Kevan, L. (1999) "Incorporation of Titanium into Mesoporous Silica Molecular Sieve SBA-15", *Chem. Mater*. **11**, 3680-3686.
10. Huang, D., Luo, G.S., and Wang, Y.J. (2005) "Using Phosphoric Acid as a Catalyst to Control the Structures of Mesoporous Titanium Dioxide Materials", *Microporous and Mesoporous Materials* **84**, 27-33.
11. Eaton, A.D., Clesceri, L.S., Greenberg, A.E. (1995) *Standard Methods for the Examination of Water and Wastewater 19th Edition*, American Public Health Association, Washington DC.
12. Masscheleyn, P.H., Delaune, R.D., Patrick, W.H. (1991) "A Hydride Generation Atomic Absorption Technique for Arsenic Speciation", *J. Environ. Qual.,* **20**, 96-100.
13. Gregg, S.J., Sing, K.S.W. (1982) *Adsorption, surface area, and porosity*, Academic Press, London.
14. Rouquerol, F., Rouquerol, J., Sing, K. (1999) *Adsorption by Powders and Porous Solids*, Academic Press, London.
15. Barrett, E.P., Joyner, L.G., Halenda, P.P. (1951) "The Determination of Pore Volume and Area Distributions in Porous Substances. I. Computations from Nitrogen Isotherms" *J. Am. Chem. Soc*. 73, 373-380.
16. Kruk, M., Jaroniec, M., Sayari, A. (1997) "Application of Large Pore MCM-41 Molecular Sieves To Improve Pore Size Analysis Using Nitrogen Adsorption Measurements" *Langmuir*, 13, 6267-6273.
17. Newalkar, B.L., Olanrewaju, J., Komarneni, S. (2001) "Direct Synthesis of Titanium-Substituted Mesoporous SBA-15 Molecular Sieve under Microwave-Hydrothermal Conditions" *Chem, Mater*. 13, 552-557.
18. Wang, W. and Song, M. (2006) "Photocatalytic Activity of Titania-Containing Mesoporous SBA-15 Silica" *Microporous and Mesoporous Mater*. 96, 255-261.
19. Shin, E.W., Han, J.S., Jang, M., Min, S.H., Park, J.K., and Rowell, R.M. (2004) "Phosphate Adsorption on Aluminum-Impregnated Mesoporous Silicates: Surface Structure and Behavior of Adsorbents", *Environ. Sci. Technol*., **38**, 912-917.

20. Yang, J., Zhang, J., Zhu, L., Chen, S., Zhang, Y., Tang, Y., Zhu, Y., and Li, Y. (2006) "Synthesis of Nano titania Particles Embedded in Mesoporous SBA-15: Characterization and Photocatalytic Activity" *J. Hazard. Materials*, **137**, 952-958.
21. McBride, M.B. (1994) *Environmental Soil Chemistry*. Oxford University Press, New York.
22. Raven, K.P., Jain, A., and Loeppert, R.H. (1998) "Arsenite and Arsenate Adsorption on Ferrihydrite: Kinetics, Equilibrium, and Adsorption Envelopes", *Environ. Sci. Technol*., **32**, 344-349.
23. Jang, M., Park, J.K., and Shin, E.W. (2004) "Lanthanum functionalized Highly Ordered Mesoporous Media: Implications of Arsenate Removal", *Microporous and Mesoporous Materials*, **75**, 159-168.